

# The thermal diffusion factor of the van der Waals binary mixture

Rolando Castillo

*Instituto de Física, UNAM, P.O. Box 20-364, D.F. 01000, Mexico*

Jorge Orozco<sup>a)</sup>

*Facultad de Ciencias, UAEM, P.O. Box 2-139, Toluca, Edo. de Mexico, 50000, Mexico*

(Received 10 December 1996; accepted 12 February 1997)

The explicit dependence of the thermal diffusion factor with respect to composition and interaction parameters for the van der Waals binary mixture is obtained in the framework of the mean-field kinetic variational theory and in the scheme of Scott and van Konynenburg. Here, we present a numerical study where the global behavior of the thermal diffusion factor is described in terms of molecular masses, sizes, and interaction parameters, along the phase diagram of this model mixture. This numerical study allows us to understand what molecular parameters modify the sign of the thermal diffusion factor. In addition, a comparison is made between the thermal diffusion factor coming from the van der Waals mixture and from the hard-sphere mixture. © 1997 American Institute of Physics. [S0021-9606(97)51019-1]

## I. INTRODUCTION

Thermal diffusion is the transport of matter associated with a thermal gradient. It may occur in both the gaseous and the liquid mixture. As a result of the thermal gradient, composition gradients subsequently appear in the mixture. Those composition gradients produce ordinary diffusion. A steady state is finally reached in which the separating effect arising from thermal diffusion is balanced by the remixing effect of ordinary diffusion. As a consequence, partial separation is observed and described by the thermal diffusion factor (TDF). Experimental results have shown in most of the cases a “normal” behavior, i.e., the heavier species in the cold region and the lighter species in the hot region. Also, there are systems with “abnormal” behavior, where the situation is the opposite. Typical values for the TDF, disregarding the sign, lie in the range of 0.3 to 1.<sup>1-6</sup> Although, they tend to infinity at the critical point of the mixture. Absolute values between 10 and 100 have been measured in the vicinity of the critical region.<sup>7</sup>

Thermal diffusion in liquids was first reported by Ludwig<sup>8</sup> and studied in detail by Soret.<sup>9</sup> For the case of gases, it was predicted independently by Enskog<sup>10,11</sup> and by Chapman,<sup>12</sup> and later confirmed with the experiments of Chapman and Dootson.<sup>13</sup> The phenomenological description of the thermal diffusion process is provided by the irreversible thermodynamics in the linear regime,<sup>14</sup> although isotope separation has been a famous application of thermal diffusion, the variety of systems studied is quite low. Therefore, it is a property quite unknown. In particular, the influence of molecular parameters on this transport property is not clear, since very few models can be explicitly developed to give the TDF in terms of molecular parameters.<sup>15</sup> By far, the most interesting property of the TDF is the origin of its sign, and how this is related to thermodynamic states and to molecular parameters of the mixture.

The purpose of this paper is to present a new method to

study the TDF of binary mixtures. There are few model mixtures for which theory can be handled almost without approximation, and at the same time they could give explicit equations relating molecular properties, in particular attractive forces, to thermal diffusion. One of those model mixtures, as will be shown here, is the van der Waals binary mixture. Therefore, here we will study the thermal diffusion for van der Waals mixtures through the mean-field kinetic variational theory (KVT I).<sup>16</sup> Points of interest will be to understand the effect of molecular masses, short-range forces (molecular volumes), and attractive potential interactions on the TDF. Of course, we will try to understand the origin of the change of sign of this property.

The phenomenological expression for the mass flux  $\mathbf{J}_i^{ph}$  (relative to the local center of mass velocity,  $i=1,2$ ), under the condition of no external forces and mechanical equilibrium ( $\nabla p=0$ ), is<sup>17,18</sup>

$$\mathbf{J}_i^{ph} = - \sum_{j=1}^2 (1 - \delta_{Lj}) D_{ij}^{CM} \nabla \rho_j - \rho D_i^T \nabla \ln T. \quad (1)$$

Here, we will confine ourselves to binary mixtures. In Eqs. (1),  $\rho$  is the mass density,  $T$  is the temperature,  $D_{ij}^{CM}$  are the mutual diffusion coefficients, and  $D_i^T$  are the thermal diffusion coefficients. Equations (1) have been written in such a way that all the gradients occurring therein are independent. The choice of the component  $L$  is arbitrary, and although it is not explicitly stated, the  $D_{ij}^{CM}$  and the  $D_i^T$  will depend upon the choice of  $L$ .<sup>17,18</sup>

As mentioned, the property more often used to describe thermal diffusion in a binary mixture is the TDF,  $\alpha_{12}$ , which is defined at stationary states as

$$\alpha_{12} = - \left[ \frac{\nabla \ln \left( \frac{\rho_1}{\rho_2} \right)}{\nabla \ln T} \right]_{\mathbf{J}_i=0} \quad (2)$$

with  $\alpha_{12} + \alpha_{21} = 0$ . The TDF is invariant to the change of reference system (center-of-mass or center-of-volume).

<sup>a)</sup>On leave from Instituto de Física, UG.

Molecular simulations have been done to obtain thermal diffusion coefficients and TDFs for Lennard-Jones liquid mixtures,<sup>19,20</sup> although most of the studies are focused on method developments. Systematic studies probably start with the work on isotopic mixtures using nonequilibrium molecular dynamics due to Kincaid *et al.*<sup>21</sup> and Hafskjold *et al.*<sup>22</sup> In the former study, the authors studied isotopic binary mixtures of particles interacting through the Lennard-Jones/spline potential. They found that the dependence of the TDF on the mass ratio in the mixture is very similar to that given by the Enskog theory. In the later study, the authors presented a study of the TDF for isotopic binary mixtures interacting through a switched Lennard-Jones potential. They found that for a stationary temperature gradient and, as a consequence, for a concentration profile: 1) The potential energy flux is small. 2) The lighter component prefers the hot side of the system. 3) The ratio of intermolecular energy transfer to kinetic energy flux increases as the density increases. This ratio also increases from the hot to the cold region in the system. The last feature is consistent with the increasing of the collision rate as density increases. In addition, they found that the contribution of the lighter component to the energy flux is predominantly kinetic energy, and this contribution increases from the cold to the hot side. The contribution of the heavier component to the energy flux is predominantly intermolecular energy transfer through molecular interactions, and it increases from the hot to the cold side.

Most of the models developed to understand the TDF come out from kinetic theory. The Chapman-Enskog solution of the Boltzmann equation yields an accurate description in the dilute gas limit.<sup>23</sup> Calculations based on the Boltzmann equation indicate that TDF is very sensitive to the intermolecular potential. For moderate and high density fluid mixtures the revised Enskog theory (RET) for hard-spheres has a prominent place, since it can give explicit calculations. Kincaid, Cohen and Lopez de Haro<sup>24</sup> using RET made a comprehensive numerical study of the TDF for the hard-sphere binary mixture. The most striking difference found by those authors, between the low-density (Boltzmann) and high-density regime, is that the region of mass ratio-diameter ratio plane for which the  $\alpha_{12}$  is strictly positive or negative, as a function of composition, is much smaller at high densities. Also,  $\alpha_{12}$  is not a monotonic function of the mole fraction, at higher densities.

More than a century ago, van der Waals developed a simple model which turned out to be extremely fruitful for describing the main properties of realistic fluids. In modern language, a rigorous formulation can be given by writing the molecular pair interaction in the form:

$$V(r) = V^S(r) + \gamma V^L(\gamma r), \quad (3)$$

where  $V^S$  refers to the short-range reference system, while  $V^L$  is the long-range part of the potential, with range  $\gamma^{-1}$ . If the properties of this model are analyzed in the limit of  $\gamma \rightarrow 0$ , the van der Waals equation, combined with the Maxwell equal-area construction, is obtained.<sup>25</sup> Besides, the van der Waals theory has been developed to understand fluid

phase equilibria in binary mixtures, revealing a rich variety of behaviors accounting for most of the types of fluid phase equilibria shown by actual mixtures, in a qualitative way.<sup>26,27</sup> This model potential has also been used to understand a long list of related problems such as the theory of capillarity,<sup>28</sup> nonuniform fluids,<sup>29</sup> interphase properties,<sup>30</sup> density fluctuations,<sup>31</sup> and the mutual diffusion coefficient.<sup>32</sup>

As mentioned, our point of departure to study the TDF of the van der Waals mixture is the KVT I.<sup>16</sup> As we shall see, explicit expressions for the thermal diffusion coefficient and for the TDF can be obtained without approximations, in terms of molecular parameters. To obtain the TDF, we also need the mutual diffusion coefficient for the van der Waals mixture. This can be obtained in the framework of the KVT I, too.<sup>32</sup> Quite recently, we presented a comprehensive study of the mutual diffusion coefficient for van der Waals binary mixture obtained with the KVT I. There, we made a numeric study devoted to understanding the dependence of the mutual diffusion coefficient in the binary mixture on molecular sizes and interaction parameters. Moreover, we related the mutual diffusion coefficient to the classification scheme devised by Scott and van Konynenburg<sup>26,27</sup> to study in a systematic way the phase equilibria of binary systems. With this classification, those authors were able to reproduce most of the known types of fluid-fluid phase equilibria observed in actual fluid mixtures. In modern language, this classification scheme relies on curvature of the free energy. The free energy curvature of a binary mixture is responsible for the specific characteristics of the equilibrium phase diagrams. The multiplicity of phases and the connectivity of their associated critical points are determined by the form of the spinodal surfaces (free energy curvature=0). The link between the mutual diffusion coefficient and the fluid phase equilibria was possible, since this coefficient in the KVT I is equal to the free energy curvature of the binary mixture, modulated by a compressibility factor, and other factors related to the dynamics of two-particle collision. Therefore, a global behavior of the mutual diffusion coefficient for the van der Waals mixture was obtained on the same basis as in the case of phase diagrams.<sup>32</sup>

The link between phase equilibria and thermal diffusion coefficient can not be done clear-cut, as in the case of the mutual diffusion coefficient, because, as it will be shown below, there are two terms in the expression of the thermal diffusion coefficient, but only one is related to the attractive tail through the chemical potential. However, for the TDF the situation is a little bit different due to its relation with the mutual diffusion coefficient. We will use along with the numerical study given below the parameters devised by Scott and van Konynenburg to describe the different types of behavior of the TDF in the binary mixture. As will be shown below this practice is useful.

The outline of the paper is as follows. In Section II, we review the KVT I, i.e., the van der Waalsian theory of transport processes, as well as the most important features of the Scott and van Konynenburg scheme. In that section, we will present the derivation of an expression for the thermal diffusion coefficient and for the TDF, in the KVT I. In Section III,

we will present the results of our numerical study and a discussion.

## II. THEORY

### A. Kinetic theory for the van der Waals mixture

The kinetic variational theory, first obtained by Karkheck *et al.*,<sup>16</sup> is defined by a set of coupled nonlinear mean-field kinetic equations given below. Those equations were derived for a system of particles interacting through a pair potential consisting of a hard-sphere part plus a smooth but otherwise arbitrary attractive tail. The set of equations for the two single particle distribution functions defined in a binary mixture  $f_i(\mathbf{r}_1, \mathbf{v}_1, t)$ , ( $i = 1, 2$ ) are the following:

$$\left[ \frac{\partial}{\partial t} + \mathbf{v}_1 \cdot \frac{\partial}{\partial \mathbf{r}_1} \right] f_i(\mathbf{r}_1, \mathbf{v}_1, t) = \mathbf{C}^{RET}(f_i, f_j) + \frac{1}{m_i} \sum_{j=1}^2 \int_{r_{12} > \sigma_{ij}} d\mathbf{r}_2 n_j(\mathbf{r}_2, t) \times g_{ij}^{HS}(\mathbf{r}_1, \mathbf{r}_2 | \{n_k\}) \frac{\partial}{\partial \mathbf{r}_1} \varphi_{ij}^{tail} \cdot \frac{\partial}{\partial \mathbf{v}_1} f_i(\mathbf{r}_1, \mathbf{v}_1, t), \quad (4)$$

where  $f_i(\mathbf{r}_1, \mathbf{v}_1, t)$  is the average number of particles of component  $i$  (with mass  $m_i$ ) at the position  $\mathbf{r}_1$ , at the velocity  $\mathbf{v}_1$ , and at time  $t$ .  $n_i = \int d\mathbf{v}_1 f_i(\mathbf{r}_1, \mathbf{v}_1, t)$ .

The Kac limit,

$$\varphi_{ij}^{tail} = \lim_{\gamma \rightarrow 0} \gamma^3 V_{ij}(\gamma r), \quad (5)$$

can be done in the mean field terms of Eqs. (4) ( $\sigma_{ij} \rightarrow 0$ ,  $g_{ij} \rightarrow 0$ ). Kinetic equations for the  $f_i$  can be obtained that embody the exact thermodynamic description of a system interacting with a potential consisting of a hard-sphere core and an infinitely weak long-range attraction, i.e., the van der Waals interaction. We shall call this theory KVT I. The collision term  $\mathbf{C}^{RET}(f_i, f_j)$  has exactly the form of that which appears in the revised Enskog theory introduced by van Beijeren and Ernst:<sup>33</sup>

$$\mathbf{C}^{RET}(f_i, f_j) = \sum_{j=1}^2 \sigma_{ij}^2 \int d\mathbf{v}_2 \int d\boldsymbol{\epsilon} (\boldsymbol{\epsilon} \cdot \mathbf{v}_{ji}) \Theta(\boldsymbol{\epsilon} \cdot \mathbf{v}_{ji}) \times [g_{ij}^{HS}(\mathbf{r}_1, \mathbf{r}_1 + \sigma_{ij} \boldsymbol{\epsilon} | \{n_k\}) f_i(\mathbf{r}_1, \mathbf{v}'_1, t) \times f_j(\mathbf{r}_1, \mathbf{v}'_2, t) - g_{ij}^{HS}(\mathbf{r}_1, \mathbf{r}_1 - \sigma_{ij} \boldsymbol{\epsilon} | \{n_k\}) \times f_i(\mathbf{r}_1, \mathbf{v}_1, t) f_j(\mathbf{r}_1, \mathbf{v}_2, t)]. \quad (6)$$

Here,  $\mathbf{v}_{ji} = \mathbf{v}_j - \mathbf{v}_i$  is the relative velocity between two particles with velocities  $\mathbf{v}_j$  and  $\mathbf{v}_i$ , respectively.  $\boldsymbol{\epsilon}$  is a unit vector directed along the line of the centers from the particle of component  $j$  to the particle of component  $i$  upon collision, and  $\Theta$  is the Heaviside step function.  $\mathbf{v}'_i$  and  $\mathbf{v}'_j$  denote the velocities of the restituting collision, which are connected to those of the direct collision  $\mathbf{v}_i$  and  $\mathbf{v}_j$  by the relations

$$\mathbf{v}'_i = \mathbf{v}_i + 2M_{ij}(\mathbf{v}_{ji} \cdot \boldsymbol{\epsilon}) \boldsymbol{\epsilon}, \quad \mathbf{v}'_j = \mathbf{v}_j - 2M_{ij}(\mathbf{v}_{ji} \cdot \boldsymbol{\epsilon}) \boldsymbol{\epsilon}, \quad (7)$$

where  $M_{ij} = m_i / (m_i + m_j)$ . The  $g_{ij}^{HS}(\mathbf{r}_1, \mathbf{r}_2 | \{n_k\})$ 's are the radial distribution functions of a binary hard-sphere mixture.

They are the same functionals of the local number densities  $\{n_k\}$ , as in the case of a binary mixture in nonuniform equilibrium.

Explicit expressions for the transport coefficients up to the Navier-Stokes level can be directly obtained by expanding the heat, the momentum and the mass fluxes to linear order in the gradients. This is done by solving Eqs. (4) in the Kac limit, in the form  $f_i = f_i^{(0)} [1 + \Phi_i]$  through the Chapman-Enskog development. Here, the  $f_i^{(0)}$  are the local Maxwell distribution functions, and  $\Phi_i \sim \mathcal{O}(\nabla)$ . The thermal conductivity and the viscosities are identical to those given in the RET.<sup>34</sup> The diffusion and thermal diffusion coefficients exhibit an explicit dependence on the tail strength, as we will show below.

We will limit our derivation to the case of the thermal diffusion of a binary mixture. Here, an explicit derivation to obtain this coefficient will be presented on the basis of the procedure developed by Lopez de Haro *et al.*<sup>34</sup> for the case of hard spheres. The starting point for our discussion will be the linearized integral equations for the  $\Phi_i$ 's in Ref. 16:

$$\sum_{j=1}^2 \sigma_{ij}^2 y_{ij} f_i^{(0)} \int d\mathbf{v}_2 f_j^{(0)} \int d\boldsymbol{\epsilon} (\boldsymbol{\epsilon} \cdot \mathbf{v}_{ij}) \Theta(\boldsymbol{\epsilon} \cdot \mathbf{v}_{ij}) \times [\Phi_j(\mathbf{v}'_2) + \Phi_i(\mathbf{v}'_1) - \Phi_j(\mathbf{v}_2) - \Phi_i(\mathbf{v}_1)] = f_i^{(0)} \left\{ (\mathbf{v}_1 - \mathbf{u}) \cdot \left[ \frac{n}{n_i} \mathbf{d}_i + \frac{\partial \ln T}{\partial \mathbf{r}} [C_i - 5/2] \right] \times \left[ 1 + \frac{8\pi}{5} \sum_{j=1}^2 \sigma_{ij}^3 y_{ij} n_j \frac{\mu_{ij}}{m_{ij}} \right] + 2 \overline{\mathbf{C}_i \mathbf{C}_i} : \frac{\partial \mathbf{u}}{\partial \mathbf{r}} \times \left[ 1 + \frac{8\pi}{15} \sum_{j=1}^2 \sigma_{ij}^3 y_{ij} n_j \frac{\mu_{ij}}{m_{ij}} \right] + 2/3 [C_i^2 - 3/2] \times \frac{\partial}{\partial \mathbf{r}} \cdot \mathbf{u} \left[ 1 - \frac{P^{HS}}{nkT} + \frac{4\pi}{3} \sum_{j=1}^2 \sigma_{ij}^3 y_{ij} n_j \frac{\mu_{ij}}{m_{ij}} \right] \right\}. \quad (8)$$

The  $y_{ij}$  are the contact values of  $g_{ij}^{eq}$ ,  $\mathbf{C}_i = \sqrt{(m_i/2kT)} \times (\mathbf{v}_1 - \mathbf{u})$ ,  $m_{ij} = m_i + m_j$ , and  $\overline{\mathbf{C}_i \mathbf{C}_i} = \mathbf{C}_i \mathbf{C}_i + (1/3) C_i^2 \vec{\mathbf{I}}$ .  $\vec{\mathbf{I}}$  is the unit dyadic and  $\mathbf{u}$  the local velocity.  $k$  is the Boltzmann constant.  $\mathbf{d}_i = \mathbf{d}_i^{HS} + \mathbf{d}_i^t$ , where

$$\mathbf{d}_i^{HS} = (n_i/n) \left\{ \beta \left( \frac{\partial \mu_i^{HS}}{\partial \mathbf{r}} \right)_T - \beta \frac{m_i}{\rho} \frac{\partial P^{HS}}{\partial \mathbf{r}} + \frac{\partial \ln T}{\partial \mathbf{r}} \times \left[ 1 + \frac{4\pi}{3} \sum_{j=1}^2 \sigma_{ij}^3 y_{ij} n_j \frac{m_i}{m_{ij}} \right] \right\} \quad (9)$$

and

$$\mathbf{d}_i^t = (n_i/n) \beta \left[ 2 \sum_{j=1}^2 a_{ij} \frac{\partial n_j}{\partial \mathbf{r}} - \frac{m_i}{\rho} \frac{\partial P^t}{\partial \mathbf{r}} \right]. \quad (10)$$

Here,  $n = \sum_{i=1}^2 n_i$ ,  $\rho = \sum_{i=1}^2 n_i m_i = \sum_{i=1}^2 \rho_i$ ,  $\beta = 1/(kT)$ . The temperature is  $T = (3/2nk)^{-1} \sum_{i=1}^2 \int d\mathbf{v}_i (1/2) m_i (\mathbf{v}_i - \mathbf{u})^2 f_i$ , and the pressure is  $P = P^{HS} + P^t$ , where

$$P^{HS} = kT \left[ n + \frac{2\pi}{3} \sum_{i,j=1}^2 \sigma_{ij}^3 y_{ij} n_i n_j \right] \quad (11)$$

and

$$P^t = \sum a_{ij} n_i n_j \quad (12)$$

with  $a_{ij} = \int V_{ij}(\mathbf{r}) d\mathbf{r}$ .

The chemical potentials are expressed as  $\mu_i(T, \{n_j\}) = \mu_i^{HS} + \mu_i^t$ , where

$$\mu_i^t = 2 \sum_{i,j=1}^2 a_{ij} n_j \quad (13)$$

and  $\mu_i^{HS}$  is the chemical potential for component  $i$  in a binary mixture of hard spheres.

As mentioned, Eqs. (8) can be solved with the same method developed for the hard-sphere mixture presented in Ref. 34, with some appropriate changes. Hence, to follow the derivation given there, we will define some variables:

$$K_i = \left[ 1 + \frac{8\pi}{5} \sum_{j=1}^2 \sigma_{ij}^3 y_{ij} n_j \frac{\mu_{ij}}{m_{ij}} \right], \quad (14)$$

$$K_i' = \left[ 1 + \frac{8\pi}{15} \sum_{j=1}^2 \sigma_{ij}^3 y_{ij} n_j \frac{\mu_{ij}}{m_{ij}} \right], \quad (15)$$

$$K_i'' = \left[ 1 - \frac{P^{HS}}{nkT} + \frac{4\pi}{3} \sum_{j=1}^2 \sigma_{ij}^3 y_{ij} n_j \frac{\mu_{ij}}{m_{ij}} \right]. \quad (16)$$

Now, Eqs. (8) can be written in the following form:

$$\begin{aligned} & \sum_{j=1}^2 \sigma_{ij}^2 y_{ij} f_i^{(0)} \int d\mathbf{v}_2 f_j^{(0)} \int d\boldsymbol{\epsilon} (\boldsymbol{\epsilon} \cdot \mathbf{v}_{ij}) \Theta(\boldsymbol{\epsilon} \cdot \mathbf{v}_{ij}) \\ & \times [\Phi_j(\mathbf{v}_2') + \Phi_i(\mathbf{v}_1') - \Phi_j(\mathbf{v}_2) - \Phi_i(\mathbf{v}_1)] \\ & = f_i^{(0)} \left\{ (\mathbf{v}_1 - \mathbf{u}) \cdot \left[ K_i [C_i - 5/2] \frac{\partial \ln T}{\partial \mathbf{r}} + \frac{n}{n_i} \mathbf{d}_i \right] \right. \\ & \left. + K_i' [2C_i C_i] : \frac{\partial \mathbf{u}}{\partial \mathbf{r}} + 2/3 K_i'' [C_i^2 - 3/2] \frac{\partial}{\partial \mathbf{r}} \cdot \mathbf{u} \right\}. \quad (17) \end{aligned}$$

Equations (17) are the same as equations (25a) of Ref. 34. The only difference relies on the definition of  $\mathbf{d}_i$ , where the tail contribution is included. Hence, following the method of solution presented there, the independent mass flux in a binary system under the condition of no external forces, i.e., mechanical equilibrium can be obtained. This mass flux, relative to the local center of mass velocity, can be obtained substituting the solution for the  $f_i$  to the first order in the gradients into the expression

$$\mathbf{J}_i(\mathbf{r}_1, t) = \int d\mathbf{v}_1 m_i (\mathbf{v}_1 - \mathbf{u}) f_i(\mathbf{r}_1, \mathbf{v}_1, t). \quad (18)$$

The most relevant steps of the derivation are presented in Appendix A. The final result is as follows:

$$\begin{aligned} \mathbf{J}_i^{(1)} = & -\frac{\rho_i}{2n^2} \sum_{j=1}^2 (1 - \delta_{jL}) \left[ \sum_{k=1}^2 d_{i,0}^{(k)} \left( E_{kj} - \frac{P_j}{P_L} E_{kL} \right) \right] \frac{\partial n_j}{\partial \mathbf{r}} \\ & - \frac{\rho_i}{2n} \left\{ \sum_{k=1}^2 \frac{d_{i,0}^{(k)}}{n} \left[ \sum_{j=1}^2 \left\{ n_k \left( \delta_{kj} + 2\rho b_{kj} \frac{m_k}{m_{kj}} y_{kj} \right) - \frac{E_{kL}}{P_L} \right. \right. \right. \\ & \left. \left. \left. \times \sum_{p=1}^2 n_p \left( \delta_{pj} + 2\rho b_{pj} \frac{m_p}{m_{pj}} y_{pj} \right) \right\} \right] - a_0^{(i)} \right\} \frac{\partial \log T}{\partial \mathbf{r}}, \quad (19) \end{aligned}$$

where the  $\mathbf{J}_i^{(1)}$  are the macroscopic mass fluxes to the first order in the gradients, relative to the local center of mass velocity,  $\rho b_{ij} = \frac{2}{3} \pi n_j \sigma_{ij}^3$ , and

$$P_i = \sum_{j=1}^2 E_{ji}, \quad (20)$$

where  $E_{ji} = (n_j/kT)(\partial \mu_i / \partial n_j)_{T, n_{k \neq j}}$ . Those functions  $P_i$  should not be confused with the pressure.

In binary mixtures, there is only one independent diffusion coefficient as well as one independent thermal diffusion coefficient. Comparing Eqs. (1) and (19) allows us to obtain expressions for the coefficients of interest here, for the van der Waals mixture in the KVT I, as follows:

(a) The thermal diffusion coefficient:

$$\begin{aligned} D_i^T = & \frac{\rho_i}{2n\rho} \left\{ \sum_{j=1}^2 \frac{d_{1,0}^{(k)}}{n} \left[ \sum_{j=1}^2 \left( n_k \left( \delta_{kj} + 2\rho b_{kj} \frac{m_k}{m_{kj}} y_{kj} \right) \right. \right. \right. \\ & \left. \left. \left. - \frac{E_{kL}}{P_L} \sum_{p=1}^2 n_p \left( \delta_{pj} + 2\rho b_{pj} \frac{m_p}{m_{pj}} y_{pj} \right) \right) \right] - a_0^{(1)} \right\}. \quad (21) \end{aligned}$$

As far as we know, this is the first derivation of the thermal diffusion factor in the KVT I.

(b) The mutual diffusion coefficient:<sup>32</sup>

$$D_{ij}^{CM} = \frac{\rho_i}{2m_j n^2} \sum_{k=1}^2 d_{i,0}^{(k)} \left[ E_{kj} - \left( \frac{P_j}{P_L} \right) E_{kL} \right]. \quad (22)$$

(c) The thermal diffusion factor can be obtained using Eqs. (21) and (22) in Eqs. (2) in the following form:<sup>34,24</sup>

$$\alpha_{ij} = k_{Ti} - k_{Tj}, \quad (23)$$

where

$$\sum_{j=1}^2 (1 - \delta_{jL}) D_{ij}^{CM} \rho_j k_{Tj} = \rho D_i^T$$

and

$$\begin{aligned} k_{TL} = & -\frac{1}{P_L n_L} \left\{ \sum_{j=1}^2 (1 - \delta_{jL}) P_j n_j k_{Tj} \right. \\ & \left. - \sum_{i=1}^2 \sum_{j=1}^2 n_i (\delta_{ij} + 2\rho b_{ij} M_{ij} y_{ij}) \right\}. \end{aligned}$$

In both Eqs. (21) and (22) the  $a_0^{(1)}$  and the  $d_{1,0}^{(j)}$  are the coefficients that appear in the Sonine polynomial expansion given by Eqs. (A8). They depend on the hard core part only. The tail contribution in Eqs. (21) and (22) comes through the

chemical potential Eqs. (13) and (20). In our derivation, the explicit dependence of the tail contribution is handled in such a way that the structure of the equations given in Ref. 34 for the case of hard spheres using RET is conserved. This is quite useful, in particular, for making comparisons between KVT I and RET. Since we need only to turn off the tail contribution to recover the TDF and the mutual diffusion coefficient as they are given in the RET. In order to obtain practical results, one restricts the number of Sonine polynomials in the expansion. We shall adopt here the convention usually called the  $N$ th Enskog approximation, i.e., only the first  $N$  Sonine polynomials are taken into account. For details see Appendix B.

Equations (22) can be transformed, straightforwardly, into the expression previously derived by Karkheck *et al.*<sup>16</sup> in terms of the Helmholtz free energy per volume  $a_v$ .

## B. The Scott and van Konynenburg scheme

Studies of fluid phase equilibria have shown that there are continuous transitions between phase diagrams that exhibit gas-liquid, liquid-liquid, and gas-gas phase separations. Critical lines are often observed to change continuously from one type of the phase separation to another. When the lines representing a single degree of freedom (pure-component vapor pressure curves, three-phase lines, critical lines, etc.) are plotted on P-T diagrams, the resulting graphs fall naturally into several different categories, providing a convenient basis for classification of the fluid phase equilibria.

A very useful classification scheme has been devised some time ago by Scott and van Konynenburg,<sup>26</sup> who used the van der Waals equation in a systematic way to study the fluid phase equilibria of binary mixtures. They characterized the mixtures by three dimensionless parameters:

$$\xi = \frac{b_{22} - b_{11}}{b_{22} + b_{11}}, \quad (24)$$

$$\zeta = \frac{\frac{a_{22}}{b_{22}^2} - \frac{a_{11}}{b_{11}^2}}{\frac{a_{11}}{b_{11}^2} + \frac{a_{22}}{b_{22}^2}}, \quad (25)$$

$$\Lambda = \frac{\frac{a_{11}}{b_{11}^2} - \frac{2a_{12}}{b_{11}b_{22}} + \frac{a_{22}}{b_{22}^2}}{\frac{a_{11}}{b_{11}^2} + \frac{a_{22}}{b_{22}^2}}. \quad (26)$$

For  $\xi=0$ ,  $\zeta$  is related to the difference in critical temperatures or pressures of the pure components, and  $\Lambda$  is related to the molar heat of mixing. The van der Waals constants  $a_m$  and  $b_m$  for the mixture depend on mole fraction  $x_i$ , as follows:

$$a_m = \sum x_i x_j a_{ij}, \text{ and } b_m = \sum x_i x_j b_{ij}. \quad (27)$$

The constants  $a_{11}$  and  $a_{22}$  measure the attractive forces between pairs of molecules of the pure components 1 and 2, respectively, and  $a_{12}$  is the corresponding parameter for the

interaction between molecules 1 and 2. The constants  $b_{ij}$  are the size parameters for the pure components and for mixed pairs, respectively. Here, in agreement with the Scott and van Konynenburg convention,<sup>26</sup> we have used the cross size parameter as

$$b_{12} = (b_{11} + b_{22})/2. \quad (28)$$

On the basis of the selected parameters  $\Lambda$  and  $\zeta$ , and on the P-T diagrams resulting from their calculations, Scott and van Konynenburg grouped fluid phase equilibria diagrams into five types (see Fig. 1). The diagrams were distinguished mainly by the configuration of the critical lines and the three-phase lines on the P-T graphs. They recognized a sixth type of diagram that occurs in some aqueous systems, but it was not among those predicted by the van der Waals equation. In the diagrams of types I and II, the gas-liquid critical line is continuous between the critical points of the pure components,  $C_\alpha$  and  $C_\beta$ . In the diagrams of type II, there is a liquid-liquid phase separation bounded by a three-phase region LLG and a liquid-liquid critical line LL. These two lines intersect an upper critical end point. In the diagrams of type IV, the liquid-liquid-gas three-phase region is bounded above and below by critical end points. In the diagrams of type III, IV and V, the gas-liquid critical line is divided into two branches. In the diagrams of type IV and V, the branch of the gas-liquid critical line originating in  $C_\beta$  terminates in an upper critical end point, while the branch originating in  $C_\alpha$  rises to a maximum pressure and passes continuously into a liquid-liquid critical line, terminating in a lower critical end point. In the diagrams of type IV, there is a second liquid-liquid phase separation at lower temperatures, with a critical line ending in a second upper critical end point. Finally, in the diagrams of type III, the branch of the critical line originating in  $C_\alpha$  rises to high pressures, sometimes passing through maximum and minimum pressures and/or a minimum in temperature.

The usefulness of the above scheme relies on the fact that it gives a qualitative description of the properties of the liquid mixtures, and very rarely yields non-physical results. The fluid phase of binary mixtures can be qualitatively discussed in terms of interaction parameters and changes of thermodynamic properties near the critical points. Therefore, a very natural extension of the work of Scott and van Konynenburg is to use this scheme to describe the behavior of the mutual diffusion coefficient and of the TDF of binary mixtures. The former has been presented quite recently by us.<sup>32</sup>

## III. THE THERMAL DIFFUSION COEFFICIENT

### A. Definition of parameters

The TDF was calculated for van der Waals liquid binary mixture through Eqs. (23) as a function of the concentration, for different thermodynamic states. Here, we will present a numerical study to understand the influence of each parameter of the model mixture on the TDF. Both the thermal diffusion and the mutual diffusion coefficients were calculated in the ninth Sonine approximation. We also present a

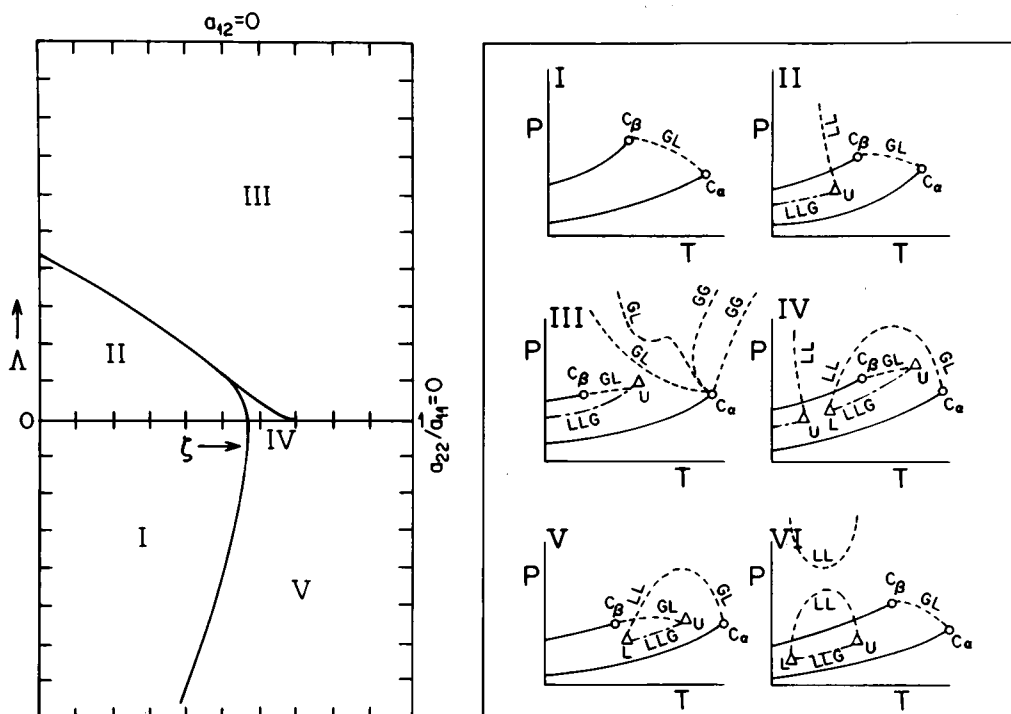


FIG. 1. Classification of Scott and van Konynenburg. (a) Values of  $\Lambda$  and  $\zeta$  defining the main regions of similar phase diagram (modified from Ref. 26). The shield region is not shown. (b) Sketches of the pressure-temperature projections of the six possible types of fluid phase equilibria exhibited by binary mixtures [modified from K. E. Gubbins, K. S. Shing, and W. B. Street, *J. Phys. Chem.* **87**, 5473 (1983)]. The vapor-pressure curves of pure components are shown as solid curves. The gas-liquid-liquid three-phase lines are shown as dash-dot, and the gas-liquid and liquid-liquid critical lines are shown dashed. The U and L are upper and lower critical end points, respectively.

comparison between the predictions of the RET (hard-sphere mixture) and of the KVT I (van der Waals mixture) to determine the effect of the attractive tail on the TDF.

There are several sets of parameters that can be used to define a binary mixture under study. We have used the following set:

$$m_1, m_2, a_{22}, b_{22}, \Lambda, \xi, \zeta, n, T, \text{ and } X_2. \quad (29)$$

Once this set is given, the other interactions parameters can be obtained with the following equations:

$$b_{11} = \frac{[1 - \xi]}{[1 + \xi]} b_{22}, \quad (30)$$

$$a_{11} = \frac{[1 - \zeta] [1 - \xi]^2}{[1 + \zeta] [1 + \xi]^2} a_{22}, \quad (31)$$

$$a_{12} = \frac{[1 - \xi] [1 - \Lambda]}{[1 + \xi] [1 + \zeta]} a_{22}. \quad (32)$$

Interpretation of the calculations is easier, if some of the above mentioned parameters are fixed for most of the calculations. As a final goal, we shall use the procedure presented here to understand the concentration dependence of the TDF, for actual binary mixtures. Therefore, we fixed some parameters close to that of simple fluids, like argon, to obtain some feeling about the influence of each parameter in actual mixtures. The fixed parameters are  $m_1 = m_2 = 6.6335 \times 10^{-23}$  g,

$a_{22} = -1.305 \text{ L}^2 \text{ At mol}^{-2}$ ,  $b_{22} = 49.79 \text{ L mol}^{-1}$ ,  $T = 168 \text{ K}$ ,  $n = 2.03 \times 10^{22} \text{ L}^{-1}$ . They will remain fixed unless otherwise explicitly mentioned.

## B. The thermal diffusion factor in the van der Waals mixture

With the theory developed above, the TDF was calculated for several binary liquid mixtures with the aim of unraveling the complex relation between the TDF and the molecular parameters of the mixture that determine its behavior. The molecular parameters  $\Lambda$ ,  $\xi$ , and  $\zeta$  were selected to fall into the different phase diagram types (I–V) of the Scott and van Konynenburg scheme. Some of our results are discussed below.

In Figs. 2 and 3, we present  $\alpha_{12}$  versus the mole fraction of component 2 ( $X_2$ ) for all the fluid mixtures types of the Scott and van Konynenburg scheme. Those calculations were done for three mass ratios of the components in the mixture ( $m_1/m_2 = 0.25, 1, \text{ and } 4$ ). Also, we included calculations for the hard-sphere binary mixture. The hard-sphere calculations just correspond to turn the attractive tails off. In general, the mass ratio is the most important parameter for determining the sign of  $\alpha_{12}$ . This will be more clear below. For  $m_1/m_2 = 0.25$   $\alpha_{12}$  is negative, for  $m_1/m_2 = 1$   $\alpha_{12}$  is close to zero, and for  $m_1/m_2 = 4$   $\alpha_{12}$  is positive no matter if there are or there are not attractive tails. Actually, our calcu-

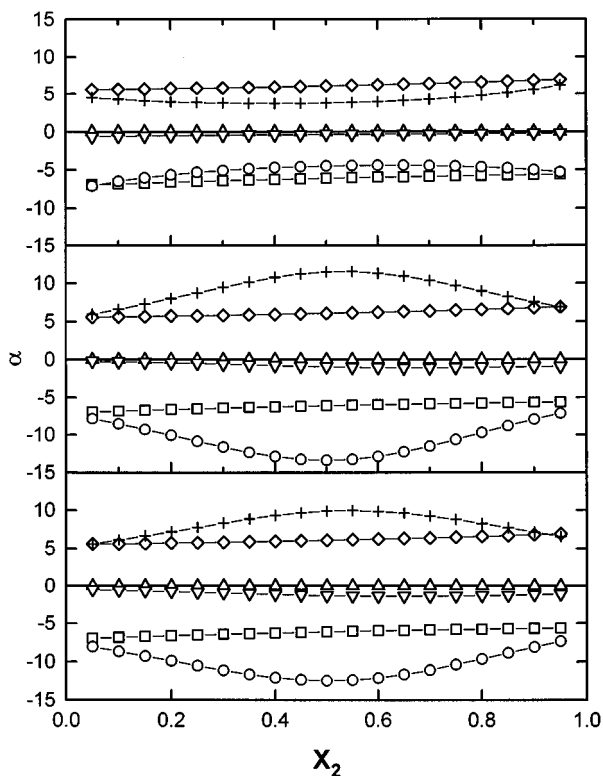


FIG. 2.  $\alpha_{12}$  versus the mole fraction of component 2 for van der Waals mixtures of types I (upper panel), II (middle panel), and III (lower panel) of the Scott and van Konynenburg scheme.  $\alpha_{12}$  is presented for three mass ratios of the components in the mixture:  $m_1/m_2=0.25$ , 1, and 4. Calculations for the hard-sphere binary mixture were also included for the same mass ratios.  $m_1/m_2=0.25$  (HS  $\square$ , VW  $\circ$ ), 1 (HS  $\triangle$ , VW  $\nabla$ ), 4 (HS  $\diamond$ , VW  $+$ ).

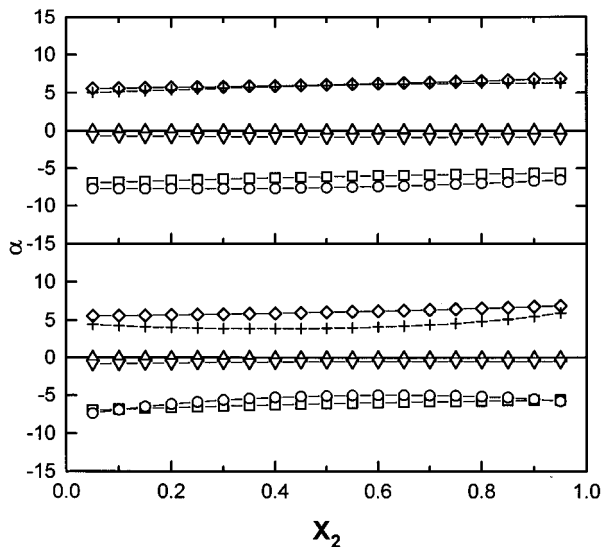


FIG. 3.  $\alpha_{12}$  versus the mole fraction of component 2 for van der Waals mixtures of types IV (upper panel) and V (lower panel) of the Scott and van Konynenburg scheme.  $\alpha_{12}$  is presented for three mass ratios of the components in the mixture. Calculations for the hard-sphere binary mixture were also included for the same mass ratios.  $m_1/m_2=0.25$  (HS  $\square$ , VW  $\circ$ ), 1 (HS  $\triangle$ , VW  $\nabla$ ), 4 (HS  $\diamond$ , VW  $+$ ).

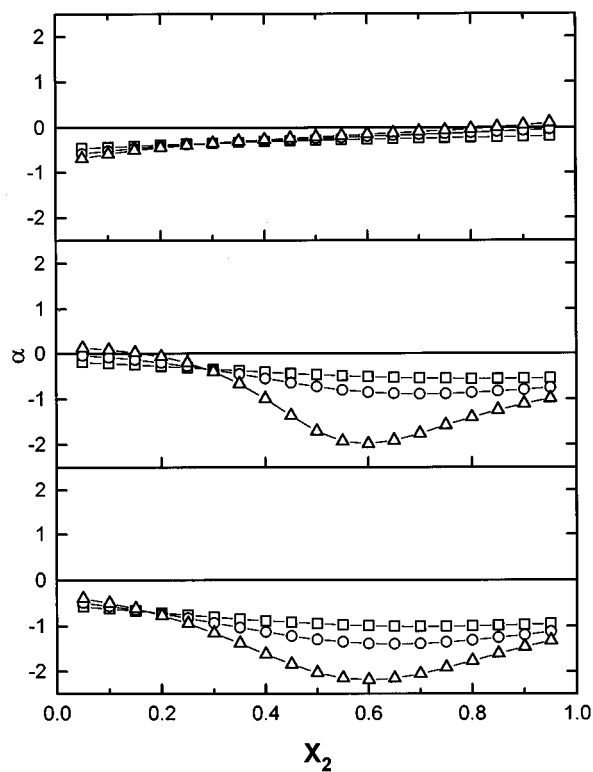


FIG. 4.  $\alpha_{12}$  versus the mole fraction of component 2 for van der Waals mixtures of types I (upper panel,  $\zeta=0.2$ ,  $\xi=0$ ;  $\Lambda=-0.1$   $\square$ ,  $\Lambda=-0.2$   $\circ$ ,  $\Lambda=-0.3$   $\triangle$ ), II (middle panel,  $\zeta=0.2$ ,  $\xi=0$ ;  $\Lambda=0.1$   $\square$ ,  $\Lambda=0.2$   $\circ$ ,  $\Lambda=0.3$   $\triangle$ ) and III (lower panel,  $\zeta=0.58$ ,  $\xi=0$ ;  $\Lambda=0.1$   $\square$ ,  $\Lambda=0.2$   $\circ$ ,  $\Lambda=0.3$   $\triangle$ ) of the Scott and van Konynenburg scheme. Here, we present how the diagrams are affected when the parameter  $\Lambda$  (cross interaction) is varied. In all those cases  $m_1/m_2=1$ .

Calculations show that the mass fraction does not determine the shape of the  $\alpha_{12}$  vs  $X_2$  diagram, but it puts a level for the sign. The attractive tails only modify the trend imposed by the mass ratio. When the mass ratio is close to one, the attractive tails do not modify in this scale range the shape of the diagrams. But, at greater mass ratios, the change due to the attractive tails is more important. For types I and V ( $\Lambda < 0$ ), the  $\alpha_{12}$  vs  $X_2$  diagrams present a curvature always in the sense of decreasing the absolute value of the TDF. On the contrary, for types II, III, and IV ( $\Lambda > 0$ ) the curvature of the  $\alpha_{12}$  vs  $X_2$  diagrams moves in the direction of increasing the absolute value of  $\alpha_{12}$ . The mass ratio dependence of  $\alpha_{12}$  obtained with the KVT I is inherited from the hard-sphere model, as it is given in the RET. As mentioned in the Introduction, Kincaid *et al.*<sup>21</sup> have shown in their molecular simulations for particles interacting through Lennard-Jones/spline potential that the mass ratio dependence of  $\alpha_{12}$  is very similar to that given in the RET. This suggests that in our procedure we have captured the correct mass ratio dependence of  $\alpha_{12}$ . The lack of symmetry in Figs. 2 and 3 is due to the molecular parameters used to define properly the different mixture types of the Scott and van Konynenburg scheme.

Figures 4 and 5 present how the TDF vs  $X_2$  diagrams are affected when the parameter  $\Lambda$  (cross interaction) is varied.

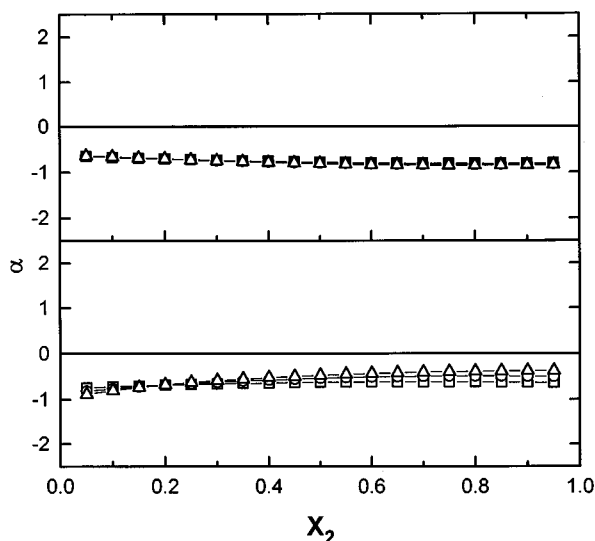


FIG. 5.  $\alpha_{12}$  versus the mole fraction of component 2 for van der Waals mixtures of types IV (upper panel,  $\zeta=0.58$ ,  $\xi=0$ ;  $\Lambda=0.015$   $\square$ ,  $\Lambda=0.025$   $\circ$ ,  $\Lambda=0.035$   $\triangle$ ) and V (lower panel,  $\zeta=0.58$ ,  $\xi=0$ ;  $\Lambda=-0.1$   $\square$ ,  $\Lambda=-0.2$   $\circ$ ,  $\Lambda=-0.3$   $\triangle$ ) of the Scott and van Konynenburg scheme. Here, we present how the diagrams are affected when the parameter  $\Lambda$  (cross interaction) is varied. In all those cases  $m_1/m_2=1$ .

In all those cases, the mass ratio was fixed equal to 1 and the parameter  $\xi=0$ . The hard-sphere calculations for  $\alpha_{12}$  in all those cases give a vanishing  $\alpha_{12}$  no matter what the concentration is. Actually, this is a test for our algorithms. A hard-sphere binary mixture of components of the same size and masses is actually a monocomponent system. Thus, the TDF must be zero. For most of the cases in the van der Waals systems, the cross interaction lowers the  $\alpha_{12}$  vs  $X_2$  diagrams to negative values. Although, in absolute value,  $\Lambda$  modifies the TDF vs  $X_2$  diagrams in a lesser extent than the mass ratio. Actually, the attractive tails change only the shape of the diagrams. The sign of  $\Lambda$  modifies the curvature of the diagrams in most of the concentration range.  $\Lambda < 0$  makes the  $\alpha_{12}$  vs  $X_2$  diagrams convex ( $\partial^2 \alpha_{12} / \partial X_2^2 < 0$ ) and  $\Lambda > 0$  makes the diagrams concave ( $\partial^2 \alpha_{12} / \partial X_2^2 > 0$ ). Although, it could be an inversion in the regions of the mixture rich in one of the components. In the latter case, the larger the  $\Lambda$ , the larger the curvature of the diagrams. This is difficult to see in Fig. 5 due to the scale, but, changing the scale, this is quite clear.

Figures 6 and 7 present the influence of the parameter  $a_{22}$  (interaction between particles of component 2) on the TDF vs  $X_2$  diagrams. Those figures show a strong sensitivity to the molecular interaction parameters  $a_{22}$ . This parameter also lowers the TDF to negative values. The more negative  $a_{22}$ , the lower the TDF. As before,  $\Lambda$  modifies the concavity of the  $\alpha_{12}$  vs  $X_2$  diagrams.  $\Lambda < 0$  (types I and V) makes them convex and  $\Lambda > 0$  (types II, III, and IV) makes them concave. As in the previous case, the test for the hard-sphere mixture (turning off the attractive tails) gives a vanishing  $\alpha_{12}$  in all the concentration range.

The dependence of the TDF on  $\zeta$  can be seen in Figs. 8 and 9 (mass ratio = 1 and  $\xi=0$ ). In most of the cases for the

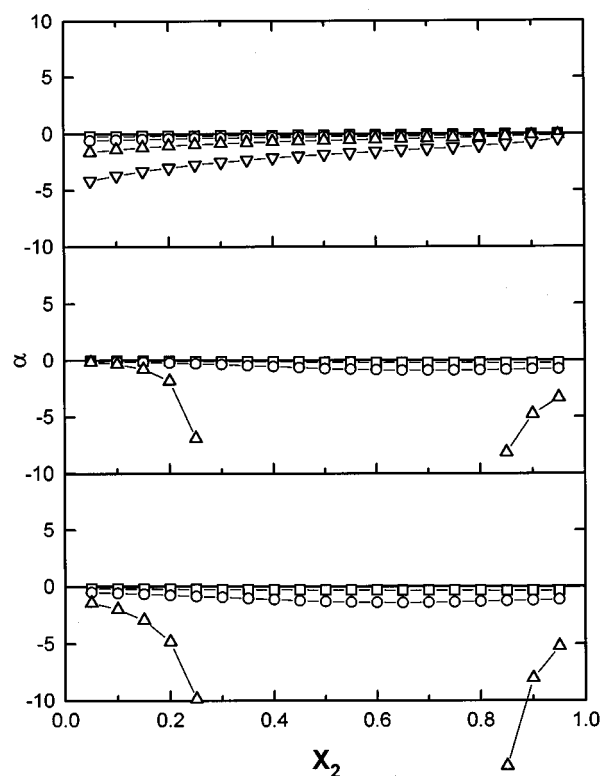


FIG. 6.  $\alpha_{12}$  versus the mole fraction of component 2 for the types I (upper panel,  $\zeta=0.2$ ,  $\Lambda=-0.2$ ,  $\xi=0$ ;  $a_{22}=-0.5$   $\square$ ,  $a_{22}=-1.3053$   $\circ$ ,  $a_{22}=-3$   $\triangle$ ,  $a_{22}=-5$   $\nabla$ ), II (middle panel,  $\zeta=0.2$ ,  $\Lambda=0.2$ ,  $\xi=0$ ;  $a_{22}=-0.5$   $\square$ ,  $a_{22}=-1.3053$   $\circ$ ,  $a_{22}=-3$   $\triangle$ ), and III (lower panel,  $\zeta=0.58$ ,  $\Lambda=0.2$ ,  $\xi=0$ ;  $a_{22}=-0.5$   $\square$ ,  $a_{22}=-1.3053$   $\circ$ ,  $a_{22}=-3$   $\triangle$ ) of the Scott and van Konynenburg scheme, showing the influence of the parameter  $a_{22}$  (interaction between particles of component 2). In all those cases  $m_1/m_2=1$ .

van der Waals mixtures, the greater the  $\zeta$ , the lower  $\alpha_{12}$ . A change of sign can be reached for a negative  $\zeta$ . In each mixture type,  $\zeta$  moves the diagrams almost in a parallel way. For some concentrations, usually close to the region rich in one component, the attractive tail can make the TDF in the van der Waals case greater than zero. It is clear from the range of variation of  $\alpha_{12}$  shown in the diagrams of Figs. 8 and 9 that  $\zeta$  modifies the  $\alpha_{12}$  diagrams less than  $\Lambda$  and  $a_{22}$ . Also here, the  $\alpha_{12}$  vs  $X_2$  diagrams of types I and V present a convex curvature for most of the concentration range.

The dependence of the TDF vs  $X_2$  diagrams on  $\xi$  can be obtained from Figs. 10 and 11. The dependence of the  $\alpha_{12}$  on the parameter  $\xi$  is important, since it can change its sign at different concentrations of the binary mixture, as well as the shape of the diagrams. For comparison, Fig. 10(a) presents the TDF for the hard-sphere binary mixture with the appropriate diameter ratio to give the same  $\xi$  values as those used for the van der Waals systems. In all the mixture types, the attractive tails modify the  $\alpha_{12}$  vs  $X_2$  diagrams in a very similar form. Comparing the van der Waals mixture and the hard sphere-mixture, the general feature is the larger  $\xi$ , the lower  $\alpha_{12}$ , for most of the concentration range. At large  $\xi$ , there is a depression in the diagrams for the van der Waals case.

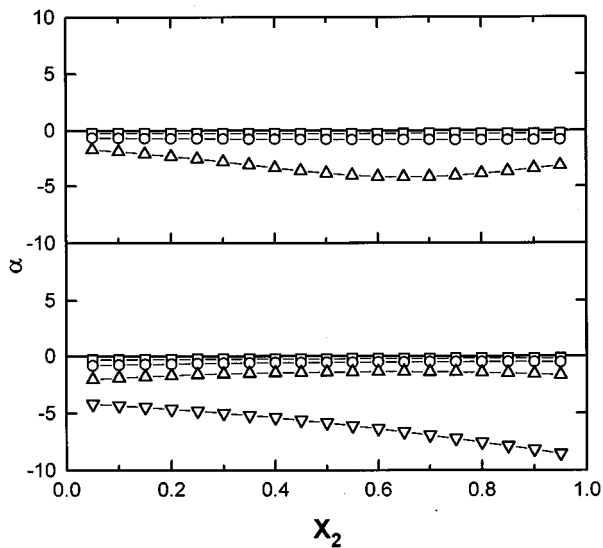


FIG. 7.  $\alpha_{12}$  versus the mole fraction of component 2 for the types IV (upper panel,  $\zeta=0.58$ ,  $\Lambda=0.025$ ;  $a_{22}=-0.5$   $\square$ ,  $a_{22}=-1.3053$   $\circ$ ,  $a_{22}=-3$   $\triangle$ ) and V (lower panel,  $\zeta=0.58$ ,  $\Lambda=-0.2$ ;  $a_{22}=-0.5$   $\square$ ,  $a_{22}=-1.3053$   $\circ$ ,  $a_{22}=-3$   $\triangle$ ,  $a_{22}=-5$   $\nabla$ ) of the Scott and van Konynenburg scheme, showing the influence of the parameter  $a_{22}$  (interaction between particles of component 2). In all those cases  $m_1/m_2=1$ .

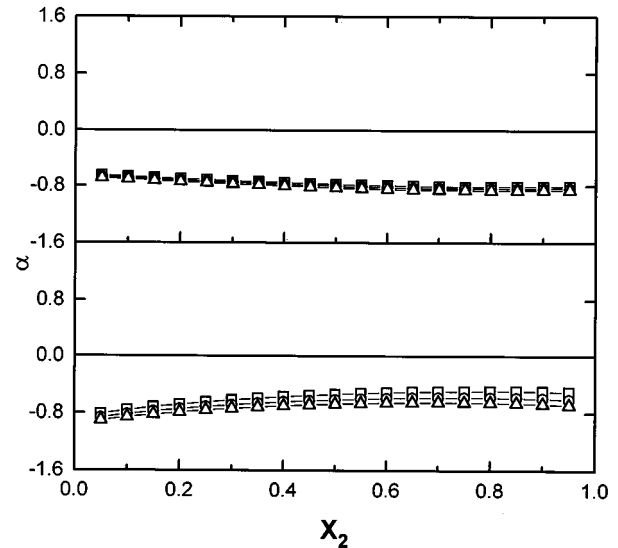


FIG. 9.  $\alpha_{12}$  versus the mole fraction of component 2 for the types IV (upper panel,  $\Lambda=0.015$ ,  $\xi=0$ ;  $\zeta=0.58$   $\square$ ,  $\zeta=0.61$   $\circ$ ,  $\zeta=0.64$   $\triangle$ ), and V (lower panel,  $\Lambda=-0.2$ ,  $\xi=0$ ;  $\zeta=0.58$   $\square$ ,  $\zeta=0.7$   $\circ$ ,  $\zeta=0.8$   $\triangle$ ) of the Scott and van Konynenburg scheme. We present here the dependence of the TDF on the parameter  $\zeta$ . In all those cases  $m_1/m_2=1$ .

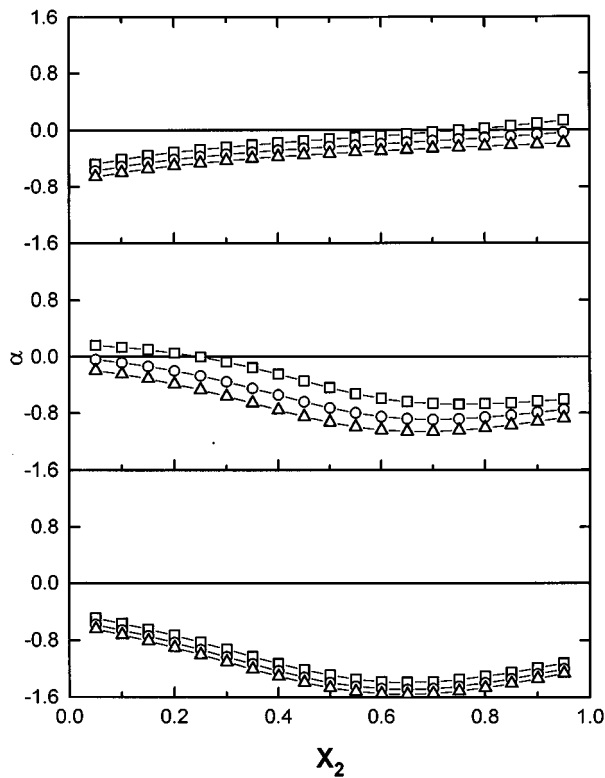


FIG. 8.  $\alpha_{12}$  versus the mole fraction of component 2 for the types I (upper panel,  $\Lambda=-0.2$ ,  $\xi=0$ ;  $\zeta=0.1$   $\square$ ,  $\zeta=0.2$   $\circ$ ,  $\zeta=0.3$   $\triangle$ ), II (middle panel,  $\Lambda=0.2$ ,  $\xi=0$ ;  $\zeta=0.1$   $\square$ ,  $\zeta=0.2$   $\circ$ ,  $\zeta=0.3$   $\triangle$ ), and III (lower panel,  $\Lambda=0.2$ ,  $\xi=0$ ;  $\zeta=0.58$   $\square$ ,  $\zeta=0.7$   $\circ$ ,  $\zeta=0.8$   $\triangle$ ) of the Scott and van Konynenburg scheme. We present here the dependence of the TDF on the parameter  $\zeta$ . In all those cases  $m_1/m_2=1$ .

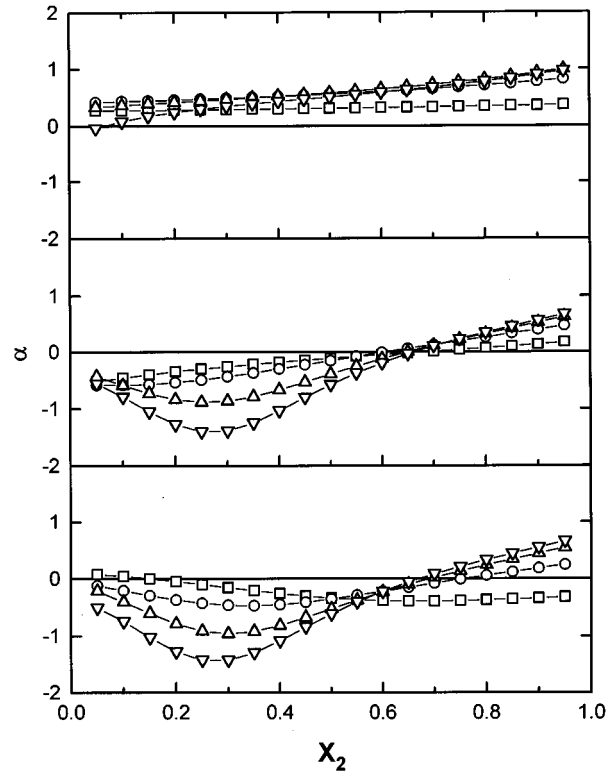


FIG. 10.  $\alpha_{12}$  versus the mole fraction of component 2, where the dependence of the TDF on  $\xi$  can be obtained ( $\xi=0.157$   $\square$ ,  $\xi=0.489$   $\circ$ ,  $\xi=0.777$   $\triangle$ ,  $\xi=0.947$   $\nabla$ ). (a) Upper panel, hard-sphere binary mixture with the appropriate diameter ratios to give the same  $\xi$  values as those used for the van der Waals systems. (b) Middle panel, mixtures of type I ( $\Lambda=-0.2$ ,  $\zeta=0.2$ ) (c) Lower panel, mixtures of type II ( $\Lambda=0.2$ ,  $\zeta=0.2$ ). In all those cases  $m_1/m_2=1$ .

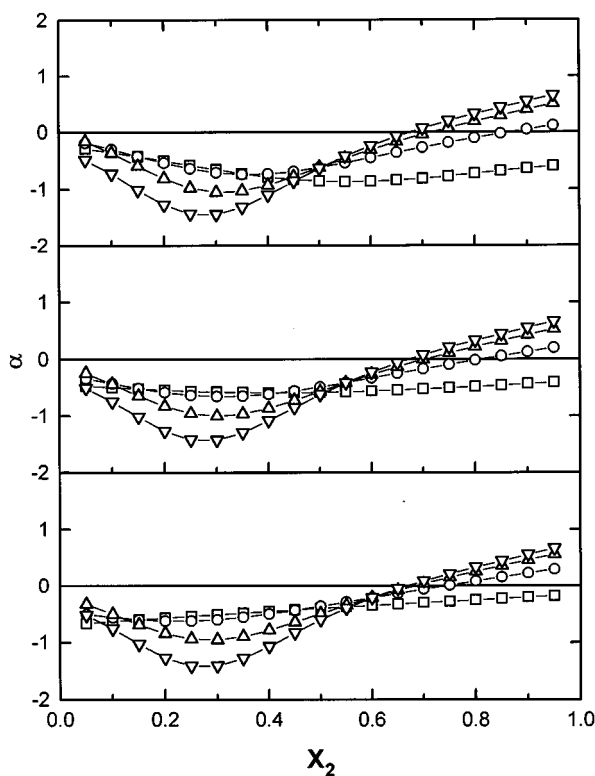


FIG. 11.  $\alpha_{12}$  versus the mole fraction of component 2, for types III ( $\Lambda=0.2$ ,  $\zeta=0.58$ ), IV ( $\Lambda=-0.025$ ,  $\zeta=0.58$ ), and V ( $\Lambda=-0.2$ ,  $\zeta=0.58$ ) of the Scott and van Konynenburg scheme, where the dependence of the TDF on  $\xi$  can be obtained ( $\xi=0.157$   $\nabla$ ,  $\xi=0.489$   $\square$ ,  $\xi=0.777$   $\circ$ ,  $\xi=0.947$   $\triangle$ ). In all those cases  $m_1/m_2=1$ .

In summary, we have presented a detailed model to study the behavior of the TDF in binary mixtures. With this model, TDFs of liquid mixtures were calculated explicitly in terms of the molecular parameters. Now, we have a clearer idea of how the different molecular parameters affect the  $\alpha_{12}$  vs  $X_2$  diagrams. Certainly, this is quite complicated. The procedure followed here can be used to correlate experimental data for actual mixtures. There are many actual systems well characterized within the Scott and van Konynenburg scheme, where an estimate for the interaction parameters can be obtained, in particular for  $\Lambda$ . We have just started to correlate some systems with good success. The appropriate combination of those effects determines the sign of  $\alpha_{12}$ . This work is underway and will be presented shortly.

#### APPENDIX A: SOLUTION TO THE INTEGRAL EQUATION FOR $\Phi_i$

Equations (17) are a set of two linear inhomogeneous integral equations for the  $\Phi_i$ . Those equations are soluble if the inhomogeneous part of the integral equations is orthogonal to the solutions of the homogeneous equations. However, the only solutions for the homogeneous equations are the conserved quantities in a binary collision. Those conserved quantities are indeed orthogonal to the inhomogeneous part of Eqs. (17). Hence, one can find the solutions and they are fixed, apart from a linear combination of solutions for the

homogeneous equations. The solution for Eqs. (17) can be made unique using the following conditions:<sup>35</sup>

$$\int f_i^{(0)} \Phi_i d\mathbf{v}_i = 0, \quad (\text{A1a})$$

$$\sum_{i=1}^s \int f_i^{(0)} \Phi_i m_i \mathbf{V}_i d\mathbf{v}_i = 0, \quad (\text{A1b})$$

$$\sum_{i=1}^s \int f_i^{(0)} \Phi_i m_i \mathbf{V}_i^2 d\mathbf{v}_i = 0. \quad (\text{A1c})$$

Here,  $\mathbf{V}_i = \mathbf{v}_i - \mathbf{u}$ .

Equations (17) are linear in the gradients of the macroscopic quantities of different tensorial character, hence it is possible to write the  $\Phi_i$  as<sup>34,35</sup>

$$n\Phi_i = -\mathbf{A}_i \cdot \frac{\partial \ln T}{\partial \mathbf{r}} - \mathbf{B}_i : \frac{\partial \mathbf{u}}{\partial \mathbf{r}} + H_i \frac{\partial}{\partial \mathbf{r}} \cdot \mathbf{u} - \sum_{k=1}^s \mathbf{D}_i^k \cdot \mathbf{d}_k. \quad (\text{A2})$$

Here, we will restrict our derivation to obtain the TDF at constant pressure. This can be performed by substituting Eqs. (A2) into  $f_i = f_i^{(0)}[1 + \Phi_i]$ , and the results must be substituted into the mass flux Eqs. (18). Therefore, an expression for the mass flux in the first order of the gradients can be written in the form

$$\mathbf{J}_i^{(1)} = -\frac{m_i}{3n} \left\{ \int d\mathbf{v}_i \mathbf{A}_i \cdot \mathbf{V}_i f_i^0 \right\} \frac{\partial \ln T}{\partial \mathbf{r}_i} - \frac{m_i}{3n} \left\{ \int d\mathbf{v}_i \sum_{k=1}^s \mathbf{D}_i^k \cdot \mathbf{V}_i f_i^0 \right\} \mathbf{d}_i. \quad (\text{A3})$$

Now, the task is to calculate the integrals in the mass flux Eqs. (A3). If Eqs. (A2) are substituted into Eqs. (17), those integrals can be obtained through the following equations:<sup>35</sup>

$$\sum_{j=1}^s \frac{n_i n_j}{n^2} I_{ij}(\mathbf{D}^k) = -\frac{f_i^0}{n_i} \left( \delta_{ik} - \frac{\rho_i}{\rho} \right) \mathbf{V}_i, \quad (\text{A4})$$

where

$$I_{ij}(\mathbf{D}^k) = \frac{y_{ij} \sigma_{ij}^2}{n_i n_j} \int \int d\boldsymbol{\epsilon} d\mathbf{v}_j (\boldsymbol{\epsilon} \cdot \mathbf{v}_{ij}) \Theta(\boldsymbol{\epsilon} \cdot \mathbf{v}_{ij}) \times f_i^0 f_j^0 (\mathbf{D}_i'^k + \mathbf{D}_j'^k - \mathbf{D}_i^k - \mathbf{D}_j^k).$$

If Eqs. (A4) are multiplied by a vector  $M$ , and integrated over velocities, then after summing over  $i$ , one can obtain expressions for Eqs. (A3), in terms of the bracket integrals:<sup>35</sup>

$$\int \sum_{i=1}^s \sum_{j=1}^s \frac{n_i n_j}{n^2} I_{ij}(\mathbf{D}^k) \mathbf{M}_i d\mathbf{v}_i = [\mathbf{D}_i^k, \mathbf{M}_i] = -\frac{1}{n_k} \int f_k^{(0)} \mathbf{V}_k \cdot \mathbf{M}_k d\mathbf{v}_k. \quad (\text{A5})$$

Here, the conditions to obtain a unique solution were used. In particular, for the case  $\mathbf{M}_i = \mathbf{D}_i^k$  and  $\mathbf{M}_i = \mathbf{A}_i$ , the integrals given in Eqs. (A5) are equal to those appearing in Eq. (A3). Thus, Eq. (A3) can be written in the form

$$\mathbf{J}_i^{(1)} = \frac{\rho_i}{3n} \left\{ [\mathbf{D}_i^l, \mathbf{A}] \frac{\partial \ln T}{\partial \mathbf{r}} + \sum_{l=1}^s [\mathbf{D}_i^k, \mathbf{D}_i^l] \mathbf{d}_l \right\}. \quad (\text{A6})$$

An explicit expression for the bracket integrals can be obtained in terms of  $\mathbf{D}_i^k(\mathbf{V}_i)$  and  $\mathbf{A}(\mathbf{V}_i)$ , if we take into account two facts. First, the integral operator of Eqs. (17) are isotropic in the velocity space, thus the  $\mathbf{D}_i^k$  and  $\mathbf{A}$  are isotropic tensors in that space, i.e.,

$$\mathbf{D}_i^k(\mathbf{V}_i) = D_i^k(V_i) \mathbf{V}_i, \quad (\text{A7a})$$

$$\mathbf{A}(\mathbf{V}_i) = A(V_i) \mathbf{V}_i. \quad (\text{A7b})$$

Second,  $D_i^k$  and  $A$  can be expanded in terms of the Sonine polynomials in the following way:<sup>34,35</sup>

$$D_i^k(V_i) = \frac{m_i}{2kT} \sum_{r=0}^{\infty} d_{i,r}^{(k)} S_{3/2}^{(r)} \left( \frac{m_i V_i}{2kT} \right), \quad (\text{A8a})$$

$$A(V_i) = \frac{m_i}{2kT} \sum_{r=0}^{\infty} a_r^i S_{3/2}^{(r)} \left( \frac{m_i V_i}{2kT} \right), \quad (\text{A8b})$$

where  $d_{i,r}^{(k)}$  and  $a_r^i$  are the Sonine coefficients, and  $S_{3/2}^{(r)}$  are the Sonine polynomials.

To calculate the bracket integrals given in Eq. (A6), we need to substitute Eqs. (A7) and (A8) into Eq. (A5). Then, this result must be multiplied by  $S_{3/2}^{(p)}$ . A working expression can be found if the orthogonality properties of the Sonine polynomials are used, as well as conditions (A1). (See Ref. 34 for details.) The bracket integrals for  $\mathbf{D}_i^k$  and  $\mathbf{A}$  can be written in terms of the Sonine coefficients in the form

$$[\mathbf{D}_i^l, \mathbf{A}] = \frac{2}{3} a_0^{(i)}, \quad (\text{A9a})$$

$$[\mathbf{D}_i^k, \mathbf{D}_i^l] = -\frac{3}{2} d_{i,0}^{(k)}. \quad (\text{A9b})$$

Equations (A6) can be written as

$$\mathbf{J}_i^{(1)} = \frac{\rho_i}{2n} \left\{ a_0^{(i)} \frac{\partial \ln T}{\partial \mathbf{r}} - \sum_{l=1}^s d_{i,0}^{(l)} (\mathbf{d}_l)_p \right\}. \quad (\text{A10})$$

Finally, using the condition

$$\sum_{i=1}^s \mathbf{d}_i = 0,$$

the expression for  $\mathbf{d}_i$  at constant pressure, can be given as

$$(\mathbf{d}_i)_p = \mathbf{d}_i = \frac{n_i}{n} \left[ \beta \left( \frac{\partial \mu_i}{\partial \mathbf{r}} \right) + \left( 1 + \frac{4\pi}{3} \sum_{j=1}^s \sigma_{ij}^3 y_{ij}^c n_j M_{ij} \right) \frac{\partial \ln T}{\partial \mathbf{r}} \right],$$

and the Gibbs-Duhem equations, Eqs. (A10), can be handled in the form given in Eqs. (19).

## APPENDIX B: EXPLICIT EXPRESSIONS FOR THE SONINE COEFFICIENTS

Substituting Eqs. (A9) and (A5) into (A4) enables us to obtain the Sonine coefficients given in Eqs. (21) and (22). (See Ref. 35 for details.) The equations obtained are

$$\sum_{j=1}^2 \sum_{q=0}^{N-1} \Lambda_{ij}^{pq} d_{j,q}^{(k)} = \frac{8}{25k} \left( \delta_{ik} - \frac{\rho_i}{\rho} \right) \delta_{p0}, \quad (\text{B1a})$$

$$\sum_{j=1}^2 \sum_{q=0}^{N-1} \Lambda_{ij}^{pq} a_q^{(j)} = \frac{4}{5} \frac{n_i}{kn} K_i \delta_{p1}, \quad (\text{B1b})$$

where

$$K_i = 1 + \frac{8}{5} \pi \sum_{j=1}^2 \sigma_{ij}^3 y_{ij} n_j \frac{m_j}{m_i + m_j}.$$

Here, the indexes are defined so that  $i=1,2$  and  $p=0,1, \dots, N-1$ . Here  $N$  denotes the  $N$ th Enskog approximation. An expression for the  $\Lambda_{ij}^{pq}$  can be given as

$$\Lambda_{ij}^{pq} = -\frac{8(m_i m_j)^{1/2}}{75k^2 T} \left\{ \delta_{ij} \sum_{l=1}^s \frac{n_l n_i}{n^2} B_{ij}^{pq'} + \frac{n_i n_j}{n^2} B_{ij}^{pq''} \right\} \quad (\text{B2})$$

with

$$B_{ij}^{pq'} = [S_{3/2}^{(p)}(C) C^{1/2} \mathbf{V}, S_{3/2}^{(q)}(C) C^{1/2} \mathbf{V}]'_{ij}$$

and

$$B_{ij}^{pq''} = [S_{3/2}^{(p)}(C) C^{1/2} \mathbf{V}, S_{3/2}^{(q)}(C) C^{1/2} \mathbf{V}]''_{ij}.$$

The bracket integrals  $[ ]'_{ij}$  and  $[ ]''_{ij}$  are defined as follows:<sup>35</sup>

$$[F, G]'_{ij} = \frac{\sigma_{ij}^{*2}}{n_i n_j} \int \int \int d\boldsymbol{\epsilon} d\mathbf{v}_j d\mathbf{v}_i (\boldsymbol{\epsilon} \cdot \mathbf{v}_{ij}) \Theta(\boldsymbol{\epsilon} \cdot \mathbf{v}_{ij}) f_i^{(0)} f_j^{(0)} \times G_i [F_i - F'_i],$$

$$[F, G]''_{ij} = \frac{\sigma_{ij}^{*2}}{n_i n_j} \int \int \int d\boldsymbol{\epsilon} d\mathbf{v}_j d\mathbf{v}_i (\boldsymbol{\epsilon} \cdot \mathbf{v}_{ij}) \Theta(\boldsymbol{\epsilon} \cdot \mathbf{v}_{ij}) f_i^{(0)} f_j^{(0)} \times G_i [F_j - F'_j],$$

where

$$\sigma_{ij}^{*2} = \sigma_{ij}^2 y_{ij}. \quad (\text{B3})$$

Equations (B1) are a set of linear equations. Those can be solved in the  $N$ th Enskog approximation to find the Sonine coefficients  $d_{j,0}^{(k)}$  and  $a_0^{(j)}$ . The coefficients can be obtained numerically solving the  $N \times N$  determinant. The Bracket integrals given in (B2) can be found through the transformation (B3). Under this transformation, the bracket integrals of Eqs. (B2) are identical to the bracket integrals of a dilute gas of hard spheres. They can be solved using the results of Ref. 36:

$$\begin{aligned}
B_{ij}^{pq'} &= 2\sigma_{ij}^{*2} \left( \frac{2kT(m_i + m_j)}{m_i m_j} \right)^{1/2} \\
&\times \sum_{n=0}^w \sum_{s=0}^{w-p} \sum_{m=0}^{w-n-s} \sum_{t=0}^1 \sum_{r=0}^{1-t} 4^n \frac{(r+s+n+t+1)!}{(n+t+1)!r!s!} \\
&\times \frac{\Gamma(p+q-2s-2n-m-r-q+1/2)}{(p-m-s-n)!(q-m-s-n)!(1-r-t)!m!} \\
&\times B_{nt}^{(1)} M_{ij}^{(1+n-r-t)} \\
&\times M_{ji}^{(p+q+t-2m-2s-n)} (M_{ij} - M_{ji})^{(m+r+2s)}, \\
B_{ij}^{pq''} &= 2\sigma_{ij}^{*2} \left( \frac{2kT(m_i + m_j)}{m_i m_j} \right)^{1/2} M_{ij}^{(q+1/2)} M_{ji}^{(p+1/2)} \\
&\times \sum_{n=0}^w \sum_{t=0}^1 4^n \frac{\Gamma(p+q-2n-t+1/2)}{(p-n)!(q-n)!(1-t)!} B_{nt}^{(2)},
\end{aligned}$$

with

$$\begin{aligned}
B_{nt}^{(1)} &= \frac{(2n+t+1)!}{2t!(2n+1)!} - 2^{t-1} \frac{(n+t+1)!}{n!t!}, \\
B_{nt}^{(2)} &= \frac{(2n+t+1)!}{2t!(2n+1)!} - \frac{1}{2} \delta_{n0} \delta_{t0}.
\end{aligned}$$

Here,  $M_{ij} = [m_i / (m_i + m_j)]$ , and  $w = \min(p, q)$ .

<sup>1</sup>P. J. Dunlop and C. M. Bignell, *Ber. Bunsenges. Phys. Chem.* **99**, 77 (1995).

<sup>2</sup>W. L. Taylor and J. J. Hurly, *J. Chem. Phys.* **98**, 2291 (1993).

<sup>3</sup>O. Ecenarro, J. A. Madariaga, J. Navarro, C. M. Santamaria, J. A. Carrion, and J. M. Saviron, *J. Phys. Condens. Matter* **2**, 2289 (1990).

<sup>4</sup>N. Y. R. Ma, D. Stanford, and A. L. Beyerlein, *J. Phys. Chem.* **87**, 5464 (1983).

<sup>5</sup>N. Y. R. Ma, and A. L. Beyerlein, *J. Phys. Chem.* **87**, 245 (1983).

<sup>6</sup>F. H. Horne and R. J. Bearman, *J. Chem. Phys.* **37**, 2857 (1962).

<sup>7</sup>R. Haase, K. H. Dücker, H. Buchner, and J. Schwinum, *Zeit. Phys. Chem.* **186**, 113 (1994).

<sup>8</sup>C. Ludwig, *Akad. Wiss. Wien. Math. Naturw.* **20**, 539 (1856).

<sup>9</sup>C. Soret, *Arch. Sci. (Geneva)* **2**, 48 (1879).

<sup>10</sup>D. Enskog, *Phys. Zeits.* **12**, 56 (1911); **12**, 533 (1911).

<sup>11</sup>D. Enskog, *Ann. Phys.* **36**, 731 (1912).

<sup>12</sup>S. Chapman, *Philos. Trans. Ser. A* **217**, 115 (1917).

<sup>13</sup>S. Chapman and F. W. Dootson, *Philos. Mag.* **33**, 248 (1917).

<sup>14</sup>F. H. Horne and R. J. Bearman, *J. Chem. Phys.* **37**, 2842 (1962).

<sup>15</sup>S. C. Yi and R. L. Rowley, *J. Chem. Phys.* **87**, 7214 (1987).

<sup>16</sup>J. Karkheck, E. Martina, and G. Stell, *Phys. Rev. A* **25**, 3328 (1982).

<sup>17</sup>S. R. De Groot and P. Mazur, *Nonequilibrium Thermodynamics* (Dover, New York, 1984).

<sup>18</sup>D. D. Fitts, *Nonequilibrium Thermodynamics* (McGraw-Hill, 1962, New York).

<sup>19</sup>R. Vogelsang and C. Hoheisel, *Phys. Rev. A* **38**, 6296 (1988).

<sup>20</sup>C. Hoheisel and R. Vogelsang, *Comput. Phys. Rep.* **8**, 1 (1988).

<sup>21</sup>J. M. Kincaid, X. Li, and B. Hafskjold, *Fluid Phase Eq.* **76**, 113 (1992).

<sup>22</sup>B. Hafskjold, T. Ikeshoji, and S. K. Ratkje, *Molec. Phys.* **80**, 1389 (1993).

<sup>23</sup>S. Chapman and T. G. Cowling, *The Mathematical Theory of Non-uniform Gases* (Cambridge University Press, Cambridge, 1952).

<sup>24</sup>J. M. Kincaid, E. G. D. Cohen, and M. Lopez de Haro, *J. Chem. Phys.* **86**, 963 (1987).

<sup>25</sup>M. Kac, P. C. Hemmer, and G. E. Uhlenbeck, *J. Math. Phys.* **4**, 216 (1963).

<sup>26</sup>P. H. van Konynenburg and R. L. Scott, *Philos. Trans. R. Soc. London* **298**, 495 (1980); R. L. Scott and P. H. van Konynenburg, *Discuss. Faraday Soc.* **49**, 87 (1970).

<sup>27</sup>D. Furman and R. B. Griffiths, *Phys. Rev. A* **17**, 1139 (1978).

<sup>28</sup>J. W. Cahn and J. E. Hilliard, *J. Chem. Phys.* **28**, 258 (1958).

<sup>29</sup>R. Evans, *Adv. Phys.* **28**, 143 (1979).

<sup>30</sup>C. Varea, A. Valderrama, and A. Robledo, *J. Chem. Phys.* **73**, 6265 (1980).

<sup>31</sup>C. Varea and A. Robledo, *J. Chem. Phys.* **75**, 5080 (1981).

<sup>32</sup>R. Castillo, C. Garza, and H. Dominguez, *J. Chem. Phys.* **99**, 9899 (1993); **100**, 6649 (1994).

<sup>33</sup>H. van Beijeren and M. H. Ernst, *Physica (Utrecht)* **68**, 437 (1973).

<sup>34</sup>M. Lopez de Haro, E. G. D. Cohen, and J. M. Kincaid, *J. Chem. Phys.* **78**, 2746 (1983).

<sup>35</sup>J. H. Ferziger and G. H. Kaper, *Mathematical Theory of Transport Processes in Gases* (North-Holland, Amsterdam, 1972).

<sup>36</sup>M. J. Lindenfeld and B. Shizgal, *Chem. Phys.* **41**, 81 (1979).